NbN–Nb–Al superconducting tunnel junctions as photon counting detectors

N. Rando,[a] P. Verhoeve, A. Poelaert, and A. Peacock
Space Science Department of the European Space Agency, Astrophysics Division, ESTEC, NL-2200 Noordwijk, The Netherlands

D. J. Goldie
Oxford Instruments, Scientific Research Division, CB4 4WY Cambridge, United Kingdom

(Received 22 December 1997; accepted for publication 23 February 1998)

Asymmetric NbN–Nb–Al–AlO_x-Al–Nb superconducting tunnel junctions have been investigated as photon counting detectors at x-ray and ultraviolet (UV)-visible wavelengths. The inclusion of a thin NbN passivation layer on the top electrode of the devices in place of the natural niobium oxides has reduced the quasiparticle loss rates, thereby enhancing the probability of multiple tunnel processes. As a consequence, the detector responsivity has increased from $900e^-$/eV, up to values in excess of $2000e^-$/eV in the temperature range 0.3–0.8 K. Such a responsivity level has allowed single photon counting performance at wavelengths as long as 700 nm and at operating temperatures as high as 830 mK. The devices show a linear response in the UV-visible range, while at 6 keV the expected nonlinearities in the energy response and moderate energy resolution similar to that found in Nb–Al junctions are observed. © *1998 American Institute of Physics.* [S0021-8979(98)10410-3]

I. INTRODUCTION

Superconducting tunnel junctions (STJs) are being extensively investigated as photon counting detectors because of their theoretically good energy resolution, high responsivity, and high count-rate capabilities. In particular, STJs are promising x-ray detectors because of their theoretically predicted energy resolution, which can be as low as 4 eV full width half maximum FWHM for 6 keV photons.[1] In addition, the large responsivity of these devices (up to 10^5e^-/eV for Ta–Al junctions, at a temperature of 0.3–0.4 K) has allowed single photon counting in the UV-visible to the near infrared.[2,3]

The large detector responsivity is due to the low energy required to break Cooper pairs in the superconducting electrodes of the junction, thereby generating free charge carriers (quasiparticles) which are then detected by tunneling across the STJ insulating barrier. The initial number of quasiparticles generated by the absorption of a photon of energy γ, is equal to $N_0=\gamma/\epsilon$. Here ϵ represents the mean charge necessary to create a quasiparticle, with $\epsilon\cong 1.7\cdot\Delta$,[1] where 2Δ is the energy gap of the superconductor absorber. In the case of niobium ($\Delta=1.55$ meV), for photons of energy $\gamma=6$ keV, we expect a total number of excess quasiparticles $N_0=2.28\times10^6e^-$.

The expected energy resolution of a STJ detector is limited by several mechanisms which, in a first approximation, can be considered as statistically independent; under this assumption, the total detector energy resolution (FWHM) can be written as:

$$\Delta E_{\mathrm{FWHM}}=2.355\cdot\sqrt{\sigma^2_{\mathrm{Fano}}+\sigma^2_{\mathrm{t}}+\sigma^2_{\mathrm{sp}}+\sigma^2_{\mathrm{el}}}\ . \tag{1}$$

In this formula $\sigma^2_{\mathrm{Fano}}=F\epsilon\gamma$ is the statistical fluctuation in the initial number of quasiparticles produced by the photoabsorption (with the Fano factor $F\cong0.22$ in Nb);[1] $\sigma^2_{\mathrm{t}}=G\epsilon\gamma$ represents the statistical fluctuations in the collected charge due to the tunneling process;[4] $\sigma^2_{\mathrm{sp}}\propto\gamma^2$ is the degradation associated with spatial nonuniformities in the detector responsivity,[5] while σ^2_{el} is the read-out electronics noise, independent of photon energy. The predicted energy resolution of an ideal detector has not yet been achieved, with the best reported ΔE of 27 eV at 6.49 keV, obtained with an Al junction.[6] The limiting factor in the measured energy resolution at photon energies above a few keV, for the rather small sized (20–50μm) junctions discussed here, is represented by a spatial nonuniformity in detector response (under the assumption $\Delta E_{\mathrm{sp}}=\alpha\gamma$, where α is typically of order 15 FWHM(eV)/keV for the detector base electrode).[5]

Spatial nonuniformities in the detector responsivity are associated with the diffusion properties of the excess quasiparticles and with loss processes taking place near the junction edges.[5] In an ideal junction the quasiparticle diffusion is not hindered by the thin films quality; in addition the only quasiparticle loss mechanism is self-recombination, occurring uniformly throughout the superconducting electrodes; finally, no performance degradation occurs as a result of the film boundaries or from losses to the leads. In a real device however, quasiparticle diffusion may be drastically affected by the thin films characteristics (such as crystalline structure, grain size, and scattering centers). The importance of these effects has been demonstrated by the results obtained through the use of low temperature scanning electron microscopy (LTSEM) on different types of Nb based STJ devices.[7,8]

One process possibly responsible for losses through qua-

[a]Electronic mail: nrando@astro.estec.esa.nl

siparticle trapping arises from the growth of natural oxides on the niobium. Experimental evidence[9] shows that the oxide growth on Nb at room temperature is characterized by two main stages: (a) the fast growth of about 0.5 nm of NbO_x ($x \leqslant 1$) acting as an interface layer; (b) slower growth of an upper Nb_2O_5 layer, stabilizing at a total thickness of about 6 nm. Recent imaging x-ray photoelectron spectroscopy (IXPS) data have substantially confirmed this picture, with a measured total thickness of the oxide layer of about 5 nm.[3] NbO is a superconductor with $T_e = 1.25$ K, while Nb_2O_5 is an insulator:[10] the presence of a lower gap superconductor such as NbO may create a quasiparticle trapping layer on top of the counter-electrode which induces charge losses and, for a nonhomogeneous oxide layer, response nonuniformities. The trapping efficiency of this very thin NbO layer will depend on the effective energy gap and coherence length, both of which will be constrained by the NbO grain structure as well as the proximization of the underlaying Nb film.

In order to reduce such losses, thereby both enhancing the detector responsivity and improving the detector energy resolution, the use of quasiparticle trapping techniques has been proposed.[11] Proximized Nb–Al devices have been successfully tested,[3,12] showing a net increase in responsivity due to the trapping and the confinement of the excess quasiparticles in the depressed energy-gap region, close to the insulating barrier. In such devices the tunneling probability as well as the quasiparticle lifetime are enhanced at the expenses of the operating temperature: the deliberate depression of the energy gap in these heavily proximized devices imposes a lower operating temperature so as to preserve the ratio Δ/KT, which determines the thermally excited quasiparticle population.[13]

The adoption of a NbN passivation layer (typically 5–10 nm thick), deposited directly on the junction counter-electrode after sputtering of the Nb–Al multilayer under ultrahigh vacuum conditions, represents an important process to eliminate the effects induced by any oxide layer.[14] In addition, the presence of a higher energy-gap material ($\Delta_{NbN} = 2.6$ meV) ensures the confinement of the excess quasiparticle in the Nb electrode, reducing the boundary effects and increasing the charge collection efficiency. High responsivities should therefore be achievable without introducing an energy-gap depression at the barrier, allowing operations at higher temperatures.

The effectiveness of the energy-gap trap is related to the ratio between the excitation time of a trapped quasiparticle and the tunnel time: if the excitation time is much longer than the tunnel time the trap is effective; if this condition is not fulfilled, then the trap can still be effective in case the quasiparticle relaxation time is much shorter than both the excitation and tunnel time.

This article presents results obtained with Nb based devices, coated by a thin NbN overlayer. In Sec. II the fabrication process and the main device characteristics are described. In Sec. III the results of experiments conducted at x-ray, UV and visible energies are presented, while in Sec. IV the experimental results are interpreted by applying theoretical considerations on the effectiveness of the quasiparticle reflection from the NbN layer.

II. DEVICE FABRICATION AND CHARACTERISTICS

A. Device fabrication

The devices under investigation have been fabricated according to a well established process described in detail elsewhere.[15] The deposition of the Nb–Al–AlO_x–Al–Nb–NbN multilayer has taken place within a single pump-down, on to a highly polished, 0.5 mm thick sapphire substrate. The base electrode, epitaxial, with residual resistivity ratio (RRR) = 58, is 100 nm thick; both the Al layers underneath and above the insulating barrier ($\cong 1$ nm thick) have a thickness of 5 nm. The polycrystalline counter-electrode is 170 nm thick, with RRR of order 5. The NbN passivation layer covering the Nb top film is 5 nm thick. Standard photolithographic techniques have been applied to isolate diamond-shaped junctions of 20 and 50 μm size. The device leads are in Nb, with a width of about 3 μm. Results from devices in which the junction leads were fabricated in NbN to reduce quasiparticle losses have been reported in Ref. 16.

The deposition of the NbN passivation layer has been performed by reactive dc sputtering in an Ar/N_2 atmosphere from a Nb target. The substrate was at ambient temperature. NbN is known to be an effective getter material thereby requiring very low deposition base pressures and high purity gases. Test runs have demonstrated transition temperatures in excess of 12 K (typically ranging between 12 and 14 K) and RRR just below unity, suggesting the deposition of polycrystalline films and a coherence length of order 3 nm (comparable with the NbN layer thickness). Under the assumption of a Bardeen–Cooper–Schrieffer (BCS) behavior, we can estimate an energy gap for the NbN film larger than 3.8 meV (to be compared with 3.0 meV of Nb), therefore adequate to ensure the reflection from the surface of quasiparticles.

B. Device characteristics

The NbN–Nb–Al–AlO_x–Al–Nb devices have been tested in both a 4 He (at $T = 1.20$ K) and a 3 He cryostat (at $T = 0.3$ K). The electrical parameters of the junctions (Table I) have been determined from the current–voltage characteristics ($I-VC$s).

The measured energy gap is similar to the value recorded for equivalent Nb–Al–AlO_x–Al–Nb devices and, consistently, the thermal contribution to the subgap current density J_{sg} (measured at a bias voltage $V = 100$ μV) plays a role only from $T > 0.8$ K. The $I-VC$ of the 20 μm device shows an interesting feature, in the form of a subgap current onset (I_{so}) peaking at a bias voltage of about 0.3 mV (Fig. 1); such a structure appears below the expected [1,0] Fiske voltage for a 20 μm diamond shaped junction (corresponding to about 0.56 mV) and close to a $V[1,0]/\sqrt{2}$ voltage. In

TABLE I. Electrical characteristics of the junctions.

R_{nn} (Ω cm^2)	1.9×10^{-6}
2Δ (meV)	2.73
J_{sg} (pA/μm^2)	0.02 (at $V = 100$ μV, $T = 0.3$ K)
J_{sg} (pA/μm^2)	8.3 (at $V = 100$ μV, $T = 1.2$ K)

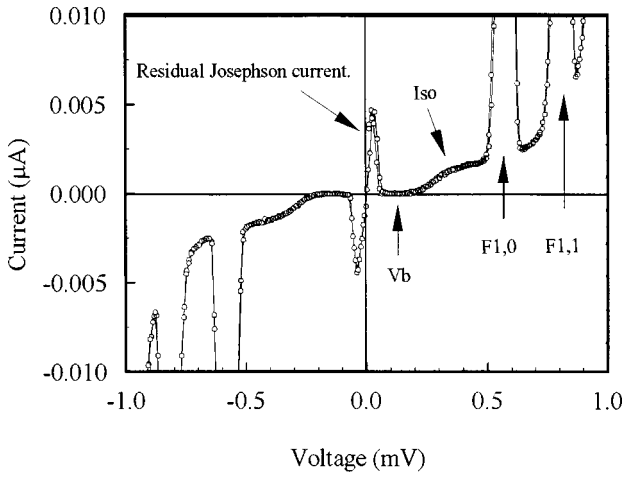

FIG. 1. Current–voltage characteristic of a 20 μm device at 0.3 K. The sub-Fiske onset peaking at about $V=0.4$ mV is clearly visible, while the two traditional Fiske steps $F_{1,0}$ and $F_{1,1}$ are also indicated, together with the typical bias point V_b. The residual Josephson current is offset from the origin due to limitations of the $I-VC$ measuring technique.

addition, the start of this current onset is temperature independent, while its intensity is reduced by increasing parallel magnetic fields, with a $1/H^2$ behavior. These indications seem to be consistent with a [1,0] Fiske mode associated with a length corresponding to the junction diagonal ($\sqrt{2}\cdot L$). Additional experimental evidence shows that the presence of the current onset depends on the device fabrication process, with particular regard to the geometric definition of the junction edges.

III. RESULTS AND ANALYSIS

A. Analysis of the x-ray performance

The devices under investigation have been tested in a pumped 4 He cryostat, at a base temperature of 1.20 K. X-ray photon illumination was provided by a 10 mCi ^{55}Fe radioactive source, emitting two line complexes, the K_α at 5895 eV and the K_β at 6491 eV. The detector chip is clamped to a copper cold finger in a vacuum chamber. A superconducting coil provides the magnetic field parallel to the junction surface which is necessary to suppress the Josephson current and to minimize the effects induced by the Fiske steps. A field of about 150 G was required to steadily operate the devices. The charge produced by each photoabsorption event was measured via a charge sensitive preamplifier operating at ambient temperature. The electronics system allows the simultaneous determination of both the integrated pulse risetime (corresponding to the decay time of the STJ current pulse) and the integrated pulse peak amplitude (corresponding to the total detected charge output).

The x-ray investigation has focused on the charge output and on the energy resolution performance, allowing a comparison with the results produced by equivalent devices, but without the NbN passivation layer. The key parameters are listed in Table II, including a comparison with nonpassivated devices of identical geometry and characteristics (RRR base=62, RRR top=4); the theoretically evaluated tunnel time τ_t for the base electrode are also included.[17]

TABLE II. Experimental results from 6 keV x-ray illumination.

Size (μm^2)	S (e−/eV)	$Q_{K\alpha}/Q_{K\beta}$	τ_t (μs)	$\Delta E_{K\alpha}$ (eV)	ΔE_n (eV)
NbN passivated devices					
20×20	730	1.080	0.87	110	11
50×50	2680	1.092	0.87	160	39
Nonpassivated devices of similar structure and characteristics					
20×20	510	1.080	0.79	150	48
50×50	920	1.095	0.79	210	80

The measured energy resolution is $\Delta E_{K\alpha}$ defined as the FWHM at 5.9 keV for the junction base electrode. In all cases the energy resolution is poor due to the low RRR of the base electrode, multiple tunneling, and most importantly, the large spatial nonuniformities. Despite this poor resolution the surface passivated devices are better, implying a reduction in at least one loss mechanism contributing to the total charge variance.

The responsivity S ($e-$/eV) of the detectors based on the measured K_α line average charge output from the bottom film has also increased significantly for the passivated devices. This does not directly translate into a corresponding improvement in the energy resolution since there exists a coupling between the two electrodes as a result of multiple tunneling.

The measured responsivity S of the passivated devices implies that the average number of tunnels per quasiparticle $\langle n\rangle$ is $\cong 7$ and 2 for the 50 and 20 μm device, respectively. These values are significantly higher than the corresponding values of $\cong 2$ and $\cong 1.3$ for the nonpassivated devices.

The linearity of the detector energy response is measured by the parameter $Q_{K\alpha}/Q_{K\beta}$, corresponding to the ratio of the measured charge output for the K_α and the K_β response of the base electrode. A perfectly linear energy response corresponds to a ratio 6491/5895=1.010. In that respect, the performance of the NbN passivated devices are as expected hardly different from those of nonpassivated junctions,[5] since both are dominated by similar rates of self-recombination.

The measured event decay times τ_d are listed in Tables III and IV for the 50 and 20 μm devices, respectively (for both the passivated and the nonpassivated devices). These decay times provide important data on the loss processes and the effectiveness of the passivation layer, particularly for the case of the 50 μm devices, where perimeter losses are less dominant. The higher value of $\langle n\rangle$ and corresponding larger decay times simply indicate a lower quasiparticle loss rate, τ_l. Note that the decay times are very similar for x-ray events originally absorbed in either the base or top electrode when $\langle n\rangle$ is large (intense multiple tunnelling). For the 20 μm device a significant difference in decay time τ_d is observed for top and bottom film events, consistent with the lower value of $\langle n\rangle$ and indicating weaker coupling between the two films. Table III and IV also include the tunneling probability $P_{i(j)}$ for a quasiparticle in the electrode $i(j)$;[4] such a probability is deduced from the average number of tunnel processes $\langle n\rangle_{i(j)}$ of a quasiparticle generated in that electrode, according to the formula:

TABLE III. Measured and derived parameters-50 μm device.

Device 50 μm	Calculated τ_t^* (μs)[a]	Calculated from Eq. (2)	Model input parameters		Model calculated values		Experimentally measured values	
film	⋯	P_{ij}	τ_t (μs)[b]	τ_l (μs)[c]	$Q(e^-)$[d]	τ_d (μs)[e]	$Q(e^-)$[d]	τ_d (μs)[e]
base	0.87	0.85	0.6	2.5	1.53×10^7	2.7	1.58×10^7	2.50
top	1.80	0.89	0.3	4.0	1.54×10^7	2.6	1.60×10^7	2.43
Nonpassivated devices of similar structure and characteristics								
base	0.87	0.87	0.4	1.2	5.4×10^6	0.81	5.4×10^6	0.83
top	1.80	0.52	0.5	0.7	4.5×10^6	0.81	4.0×10^6	0.80

$$\langle n\rangle_i = P_i\cdot(1+P_j)/(1-P_i\cdot P_j). \quad (2)$$

In addition to the experimentally measured parameters, Tables III and IV summarize the results obtained from a theoretical model of the STJ, in relation to the listed input parameters. The model is based on a simplified set of the Rothwarf and Taylor equations[18] and has been discussed in detail in Ref. 5. An acceptable fit between the observed and the calculated values can only be obtained assuming tunnel times τ_t considerably shorter than what is predicted on the basis of the device geometry ($\tau_t^{\text{top}}=1.8$ μs, $\tau_t^{\text{base}}=0.9$ μs).[17]

For comparison, the results of the same model are shown in Tables III and IV for the nonpassivated devices discussed above.[16] The significant shortening of the tunnel time for the top film of the passivated device (0.3 μs for the 50 μm device) compared to that predicted from the simple formulae of Ref. 17 (1.8 μs) implies that the NbN passivated layer is responsible for an effective shortening of the tunneling time. The difference between the tunneling times as determined from Ref. 17 may reflect uncertainties in the effective confinement length in the niobium as well as the coupling between the base and the top film. This situation arises in both the nonpassivated and passivated cases.

A significant increase in the top film tunnel probability P_{ij} has occurred for the passivated devices compared with the nonpassivated device while the overall loss time τ_l is significantly longer in the passivated case.

Good agreement exists between the measured and the model decay times. Comparison of these decay times between the passivated and the nonpassivated devices clearly supports the role of the NbN passivation layer in increasing the quasiparticle lifetime in the top electrode, thereby enhancing the tunneling probability and the actual detector responsivity.

B. Analysis of the visible-UV performance

The responsivity levels recorded for x rays are such as to allow single photon counting performance at UV and visible wavelengths. A typical spectrum at $\lambda=300$ nm is presented in Fig. 2. Simple signal-to-noise (S/N) estimates show that the detection threshold corresponding to a mean signal five times larger than the electronics noise (typically $\sigma_n=900e^-$ rms) is in excess of 700 nm (50 μm junction). An important issue is the capability of these detectors to operate at higher temperatures than those required by Ta based or heavily proximized Nb–Al devices.[3,10,12]

In order to verify this aspect, the detectors have been tested in a 3 He cryostat, at temperatures ranging from 0.3 to 1.0 K, while illuminated by UV and visible radiation, from 225 to 700 nm. The illumination takes place through the sapphire substrate (back-illumination mode), via an optical fiber and a monochromator, thus only stimulating the base electrode. Figure 3 shows the S/N (defined as $\langle Q(\lambda)\rangle/\sigma_n$ at $\lambda=470$ nm) of the 50 μm junction as a function of the applied bias voltage and at different temperatures, ranging from 300 to 830 mK. It is interesting to observe that while the responsivity of the 20 μm device is independent of temperature ($S\cong600e^-/\text{eV}$), the 50 μm device has a responsivity increasing with temperature ($+62.5\%/\text{K}$ at a bias $V=0.18$ mV). In the case of the 50 μm device, the responsivity in the visible at 300 mK is a factor of 3 lower than the

TABLE IV. Measured and derived parameters -20 μm device.

Device 20 μm	Calculated τ_i^* (μs)[a]	Calculated from Eq. (2)	Model input parameters		Model calculated values		Experimentally measured values	
film	⋯	P_{ij}	τ_t (μs)[b]	τ_l (μs)[c]	$Q\ (e^-)$[d]	τ_d (μs)[e]	$Q\ (e^-)$[d]	τ_d (μs)[e]
base	0.87	0.61	0.6	1.1	4.4×10^6	0.86	4.3×10^6	0.77
top	1.80	0.73	0.3	0.8	4.6×10^6	0.81	4.7×10^6	0.74
Nonpassivated devices of similar structure and characteristics								
base	0.87	0.57	0.4	0.8	3.2×10^6	0.51	3.0×10^6	0.53
top	1.80	0.57	0.4	0.4	2.7×10^6	0.36	2.9×10^6	0.47

[a] τ_t^* (μs) is the tunnel time calculated with formula of Ref. 17.
[b] τ_t (μs) is the tunnel time used in the model as input parameter.
[c] τ_l (μs) is the loss time.
[d] $Q(e^-)$ is the measured or calculated mean charge output.
[e] τ_d (μs) is the decay time.

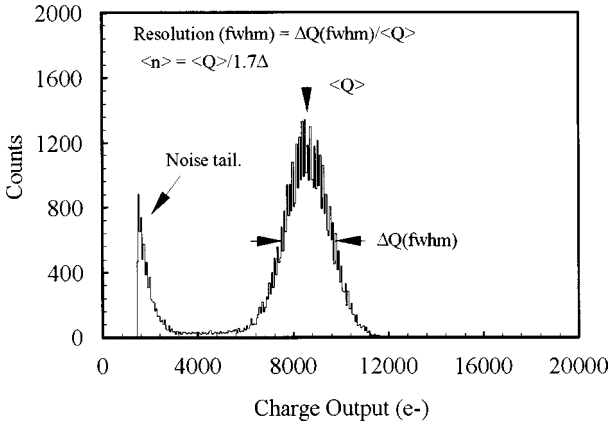

FIG. 2. The charge spectrum of a 50 μm passivated device operated at $T=830$ mK, when back-illuminated by monochromatic photons at a wavelength $\lambda=300$ nm. The bias voltage was $V_b=0.18$ mV, with an applied magnetic field $B=156$ G.

value recorded at x-ray energies. Thus the overall responsivity dependence on photon energy and device size would appear different in these passivated devices compared to non-passivated yet heavily proximized devices.[2,3] The noise performance is dominated by the read-out electronics and ranges between 600 and 800e^- rms, increasing with T only above 820 mK, when the $I-VC$s begin to change.

Due to the better S/N the UV-visible measurements have focused on the 50 μm device and on its performance at an operating temperature of 830 mK. The bias voltage was 180 μV, while the applied magnetic field was 160 G. Figure 4 shows the energy response linearity in the range 1.8–6.2 eV ($\lambda=200-700$ nm). The solid line represents the fit to a linear relationship between measured charge output and photon energy, showing a detector responsivity of 2122e^-/eV. The deviations from linearity are smaller than 0.5% over the complete energy range; this result is consistent with previously reported results and justified by both the small wavelength range explored and the low energies involved.[5]

The energy resolution is presented in Fig. 5, showing the measured FWHM resolution (circles) as a function of the

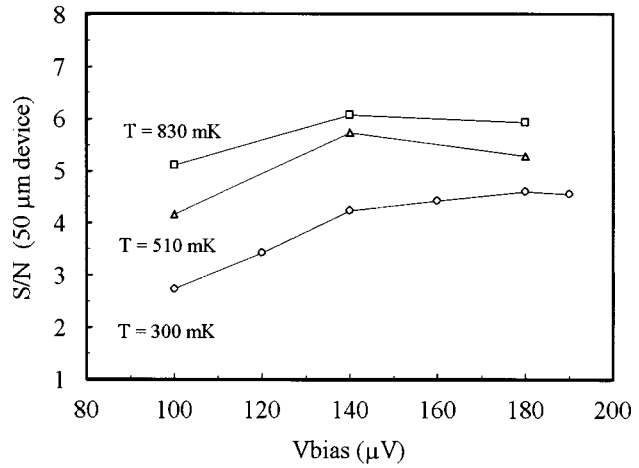

FIG. 3. Signal to noise ratio for the 50 μm device as a function of the applied bias voltage at various operating temperatures. The applied magnetic field was 160 mG.

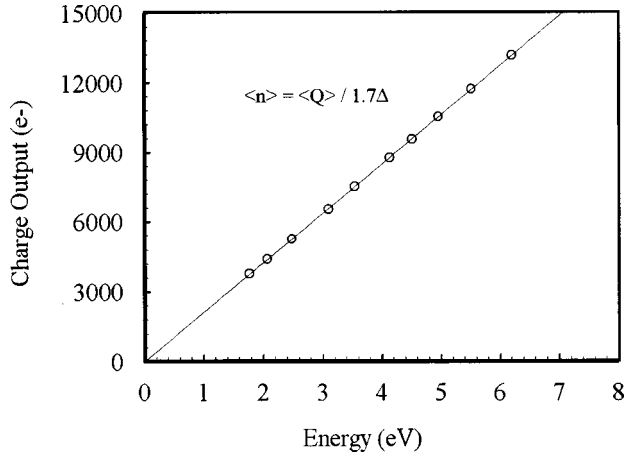

FIG. 4. Measured mean charge output $\langle Q\rangle$ as a function of the photon energy E. The solid line represents a linear best fit of the form: $Q=S\cdot E+\alpha$, where $S=1122e^-$/eV represents the detector responsivity and $\alpha=-185e$- is a constant, related to the analog-to-digital converter (ADC) electronics offset.

photon energy in the range 1.8–6.2 eV ($\lambda=200-700$ nm). The plot includes the intrinsic detector FWHM (diamonds), corresponding to the combined effect of Fano, tunnel, and spatial nonhomogeneity effects, based on Eq. (1), with $\langle n\rangle$ derived from the optical data. The solid line represents the theoretically expected detector FWHM under the assumption of Fano and tunnel limited performance: the curve is obtained with $G=1.85$, as calculated from the tunnel probability $P1$ and $P2$ (Table III). The dashed line corresponds to the expected energy resolution including the Fano limit, the tunnel contribution, and the spatial nonhomogeneities, under the assumption that $\Delta E_{sp}=\alpha\gamma$, with $\alpha=0.0339$ FWHM (eV)/eV. Such an assumption is consistent with the measured FWHM resolution at 6 keV (FWHM of about 200 eV at 5895 eV).

It is worth comparing the performance of the NbN passivated devices with the results obtained from Ta based STJ's at an operating temperature of about 0.3 K.[19] Ta based

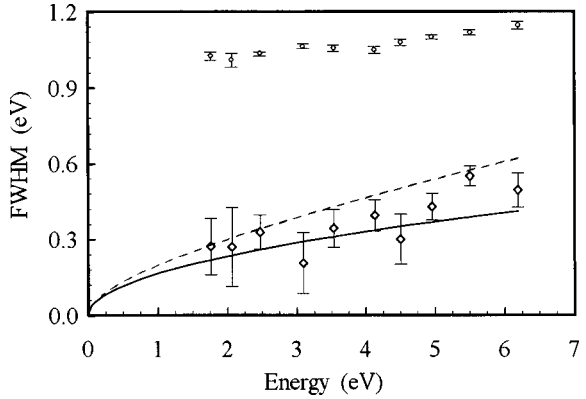

FIG. 5. The energy resolution as a function of the photon energy. The circles represent the observed energy resolution. The squares represent the detector intrinsic resolution ($\Delta E_i=\sqrt{\Delta E_m^2-\Delta E_{el}^2}$). The solid line represents the predicted Fano and tunnel limited energy resolution, while the dotted line indicates the same but with additional contributions from spatial nonhomogeneities.

devices have shown responsivities of the order $10^4-10^5 e^-/\text{eV}$, with an average number of tunnel processes ranging from $\langle n\rangle=6$ (10 μm junction) to $\langle n\rangle=190$ (100 μm junction). Due to the very high responsivity, the minimum detectable photon energy is of order 0.2 eV (corresponding to $\lambda\approx 6$ μm). The measured energy response linearity is also very good (within 0.6%), while the typical measured FWHM energy resolution at $\lambda=500$ nm ($E=2.48$ eV), is of the order 0.2 eV. The superior performance of the Ta based devices is clearly related to the smaller energy gap and the longer characteristic time τ_0 of this superconductor, but they are only obtained at considerably lower operating temperatures ($T<400$ mK).

IV. EFFECTIVENESS OF QUASIPARTICLE CONFINEMENT

The photon absorption is more likely to occur in Nb rather than in the very thin (5 nm) NbN or Al layers: in fact the $1/e$ absorption depth in Nb for photons with λ between 200 and 1000 nm is about 10 nm while at 6 keV it is about 3.62 μm. Hence we can assume that the quasiparticles will reach the low energy states available in Nb, and be confined. The confinement is effective if the confined quasiparticles tunnel before they are excited (with the absorption of a phonon) to an energy higher than the energy gap of NbN, Δ_{NbN}. In case the excitation is faster than the tunneling process, the confinement can still be effective if the excited quasiparticles relax rapidly back to a low energy state. If the relaxation process is slower than the excitation process, then the confinement is not effective.

The characteristic times to compare are the tunnel time from the top film, τ_t, given in Tables III and IV of Sec. III, and the excitation time $\tau_{\text{exc}}(\Delta_{\text{Nb}}\rightarrow\Delta_{\text{NbN}})$ of a quasiparticle of energy equal to the energy gap of Nb, Δ_{Nb}, to an energy equal to or larger than Δ_{NbN}. This time is given by:[20]

$$\tau_{\text{exc}}^{-1}(\Delta_{\text{Nb}}\rightarrow\Delta_{\text{NbN}})\approx \frac{1}{\tau_{0,\text{Nb}}(kT_{c,\text{Nb}})^3 d_{\text{Nb}}} \times\int_{\text{Nb}}\int_{\Delta_{\text{NbN}}-\Delta_{\text{Nb}}}^{\Omega_{D,\text{Nb}}}\Omega^2\,\frac{1}{\exp(\Omega/kT)-1} \times\left[N(x,\Delta_{\text{Nb}}+\Omega) -\frac{\Delta_p(x)}{\Delta_{\text{Nb}}}P(x,\Delta_{\text{Nb}}+\Omega)\right]d\Omega\,dx. \tag{3}$$

In this equation, $\tau_{0,\text{Nb}}$ is the characteristic time of Nb as defined by Kaplan;[21] $T_{c,\text{Nb}}$ is the critical temperature of Nb (9.25 K); T is the device operating temperature; d_{Nb} is the thickness of the Nb layer; $N(x,E)$ is the quasiparticle density of states as a function of position x and energy E, $P(x,E)$ is the Cooper pair density of states; $2\Delta_p(x)$ is the Copper pairs potential. Note here x is the direction perpendicular to the barrier of the STJ. The integration is over the energy Ω of the phonon absorbed by the quasiparticle of energy Δ_{Nb}. In our case, we are interested in any phonons of energy larger than $\Delta_{\text{NbN}}-\Delta_{\text{Nb}}$ such that the quasiparticle can be lifted up to an energy higher than or equal to Δ_{NbN}. The factor Ω^2 comes from the assumption of a Debye spectrum for the phonons, and therefore the integration over Ω is limited to the Debye energy in Nb $\Omega_{D,\text{Nb}}$. The factor with the exponential term is the Bose factor for the phonons; the Fermi factor for the quasiparticles is neglected, due to the high energies involved. The integration over x is limited to the Nb layer (confined quasiparticles).

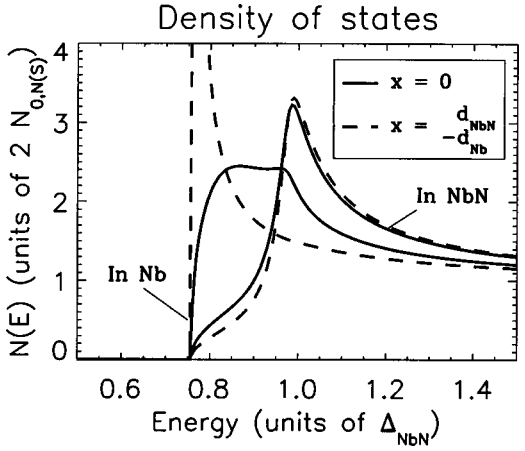

FIG. 6. Quasiparticle density of states as a function of energy. The density of states is shown in Nb at $x=0$, corresponding to the Nb/NbN interface (solid line) and at $x=-d_{\text{Nb}}$, corresponding to the Nb/Al interface (dotted line). In NbN the density of states is shown at $x=0$, corresponding to the Nb/NbN interface (solid line) and at $x=d_{\text{NbN}}$ corresponding to the NbN/vacuum interface (dotted line). The energy is in units of Δ_{NbN}. Inside the Nb film, the density of states is almost BCS-like, with a energy gap equal to the energy gap of bulk Nb.

The pair potential and the densities of states can be calculated based on the model described in Ref. 22, as a function of position and energy. This model uses the proximity effect parameters

$$\gamma_m=\frac{\rho_{\text{NbN}}\xi_{\text{NbN}}}{\rho_{\text{Nb}}\xi^*_{\text{Nb}}};\quad \gamma_B=\frac{R_B}{\rho_{\text{Nb}}\xi^*_{\text{Nb}}}, \tag{4}$$

with $\rho_{\text{Nb(NbN)}}$ the normal state specific resistivity of Nb (NbN), ξ_{NbN} the coherence length in NbN, while the reduced coherence length in Nb is

$$\xi^*_{\text{Nb}}=\xi_{\text{Nb}}\sqrt{T_{c\text{Nb}}/T_{c,\text{NbN}}} \tag{5}$$

and R_B the resistance of the Nb/NbN interface multiplied by its area. Further parameters needed are the thickness of Nb and NbN in units of the coherence lengths. Data from Sec. II (RRR and coherence lengths) imply for $\gamma_m\approx 0.5$. In order to match the energy gap predicted by the model to the observed energy gap, γ_B is chosen equal to 3. These values, under the assumption of $T_c=12$ K for NbN, correspond to a worst case scenario with respect to the effectiveness of the confinement. The values imply $R_B\approx 5.3\times 10^{-16}$ Ω m^2, i.e., a resistance of 1.3 $\mu\Omega$ for the Nb/NbN interface of a 20×20 μm^2 device.

The quasiparticle density of states is shown as a function of energy and position in Fig. 6. On the basis of this density of states and of the equivalent one for the Cooper pairs, using Eq. (3), we obtain an excitation time of about 0.4 μs for a quasiparticle of energy Δ_{Nb} confined in Nb. The excitation process is only slightly slower than the tunneling process reported in Tables III and IV (0.3 μs in the top electrode). In this regime we therefore need to estimate the

relaxation rate of excited quasiparticles, down to an energy lower than Δ_{NbN}. The relaxation time $\tau_{rel}(\Delta_{NbN})$ of a quasiparticle located in Nb is given by:[20]

$$\tau_{rel}^{-1}(\Delta_{NbN}) \approx \frac{1}{\tau_{0,Nb}(kT_{c,Nb})^3 d_{Nb}} \times \int_{Nb}\int_{0}^{\Delta_{NbN}-\Delta_{Nb}} \Omega^2 \frac{\exp(\Omega/kT)}{\exp(\Omega/kT)-1} \times \left[N(x,\Delta_{NbN}-\Omega) - \frac{\Delta_p(x)}{\Delta_{NbN}} \times P(x,\Delta_{NbN}-\Omega) \right] d\Omega\, dx. \quad (6)$$

A similar equation holds for excited quasiparticles located in NbN, where the characteristic time, the critical temperature, the layer thickness, and the integration over x are changed to the appropriate values for NbN. The characteristic time $\tau_{0,NbN}$ for NbN can be calculated from $\tau_0=(1+\lambda)\cdot\hbar/2\pi\cdot b\cdot(kT_c)^3$,[19] where b is the constant of proportionality in the low frequency quadratic form for $\alpha^2F(\omega)=b\Omega^2$, the electron-phonon spectral function, and λ is the electron-phonon coupling constant. The tunneling measurements of $\alpha^2F(\omega)$ vs Ω for NbN obtained by Kihlstrom *et al.*[23] have been fitted to obtain b. This gives $\tau_{0,NbN}=55\pm5$ ps for $T_c=12$ K and $\tau_{0,NbN}=35\pm3$ ps for $T_c=14$ K taking $\lambda=1.46\pm0.10$.

The phonon energy is integrated in Eq. (6) up to $\Delta_{NbN}-\Delta_{Nb}$ which is the maximum energy phonon emitted as a quasiparticle scatters to energies below the gap of NbN. The relaxation times apply strictly to quasiparticles of energy equal to Δ_{NbN}. We calculate a relaxation time of 4.15 ns in Nb and 8 ± 2 ns for quasiparticles in the NbN, where the error reflects the uncertainty in the transition temperature. The relaxation rate is some 50–100 times faster than the excitation rate and 40–70 times faster than the tunneling rate. We conclude that the large majority of the quasiparticles are confined in the Nb film before tunneling.

V. CONCLUSIONS

The role of a 5 nm NbN passivation layer deposited on top of a high quality Nb–Al–AlO_x–Al–Nb junction has been investigated by exposing diamond-shaped, 20 and 50 μm devices to x-ray and UV-visible photons. The experimental results have indicated a net increase of the detector responsivity, from 900 (devices without passivation layer) to $2600e^-$/eV (50 μm device). Such an increase in responsivity is consistent with a reduction of the quasiparticle loss rate in the top electrode and with a corresponding increase in the measured decay time. This interpretation is confirmed by theoretical considerations on the effectiveness of the quasiparticle confinement mechanism. As expected, the detector operating temperature is not affected, allowing single photon counting operations up to a wavelength $\lambda=700$ nm and at 0.83 K. Such an operating temperature, while not compatible with the performance of a mechanically pumped 4 He system, is considerably higher than the one required by Ta based or heavily proximized Nb–Al devices (0.3–0.5 K). The responsivity of the 50 μm device at visible wavelength has been found to be dependent on temperature, from $1500e^-$/eV at 0.3 K to $2100e^-$/eV at 0.85 K, indicating the role of thermal excitation in the trapping process. The energy response between 200 and 700 nm has been found to be linear within 0.5%, while the measured FWHM energy resolution over the same wavelength range corresponds to about 1.1 eV. The effectiveness of the quasiparticle confinement is found to be consistent with a theoretical estimate of the excitation and relaxation times in Nb and NbN.

ACKNOWLEDGMENTS

The authors wish to acknowledge the valuable support of D. Glowacka and M. Wallis for the device fabrication. The assistance of Tim Harper for diagnostic activities is also acknowledged. A. Golubov has provided valuable input into the analysis of the quasiparticle confinement effectiveness. Valuable support on the data acquisition electronics has been provided by Axel van Dordrecht.

[1] N. Rando, A. Peacock, A. van Dordrecht, C. Foden, R. Engelhardt, B. G. Taylor, J. Lumley, C. Pereira, and P. Gare, Nucl. Instrum. Methods Phys. Res. A **313**, 173 (1992).
[2] A. Peacock, P. Verhoeve, N. Rando, A. van Dordrecht, B. G. Taylor, C. Erd, M. A. C. Perryman, R. Venn, J. Howlett, D. J. Goldie, J. Lumley, and M. Wallis, Nature (London) **381**, 135 (1996).
[3] A. Peacock, P. Verhoeve, N. Rando, A. van Dordrecht, B. G. Taylor, C. Erd, M. A. C. Perryman, R. Venn, J. Howlett, D. J. Golie, J. Lumley, and M. Wallis, J. Appl. Phys. **81**, 7641 (1997).
[4] D. J. Goldie, P. L. Brink, C. Patel, N. E. Booth, and G. L. Salmon, Appl. Phys. Lett. **64**, 3169 (1994).
[5] P. Verhoeve, N. Rando, J. Verveer, A. Peacock, A. van Dordrecht, P. Videler, M. Bavdaz, D. J. Goldie, T. Lederer, F. Scholtze, G. Ulm, and R. Venn, Phys. Rev. B **53**, 809 (1996).
[6] P. Hettl, G. Angloher, M. Bruckmayer, F. v. Felitzsch, J. Jochum, H. Krauss, and R. L. Mossbauer, Proceedings of LTD-7, Munchen, Germany, 1997, pp. 20–24.
[7] P. A. J. de Korte, M. L. van den Berg, M. P. Bruijn, J. Gomez, F. Kiewiet, H. L. van Lieshout, O. J. Luiten, C. G. S. Brons, J. Flokstra, and A. W. Hamster, Proc. SPIE **2808**, 506 (1996).
[8] J. Martin, S. Lemke, R. Gross, R. P. Huebener, P. Videler, N. Rando, T. Peacock, P. Verhoeve, and F. A. Jansen, Nucl. Instrum. Methods Phys. Res. A **370**, 88 (1996).
[9] M. Grundner and J. Halbritter, Surf. Sci. **136**, 144 (1984).
[10] *Handbook of Chemistry and Physics*, edited by R. C. Weast and D. R. Lide (CRC, Boca Raton, FL, 1989–1990).
[11] N. E. Booth, Appl. Phys. Lett. **50**, 293 (1987).
[12] C. A. Mears, S. E. Labov, and T. A. BarfKnecht, J. Low Temp. Phys. **93**, 561 (1993).
[13] J. Bardeen, L. N. Cooper, and J. R. Schrieffer, Phys. Rev. **108**, 1175 (1957).
[14] R. Cristiano, E. Esposito, L. Frunzio, S. Pagano, L. Parlato, G. Peluso, G. Pepe, U. Scotti di Uccio, H. Nakagawa, M. Aoyagi, H. Akoh, and S. Takada, Appl. Phys. Lett. **67**, 3340 (1995).
[15] M. Gurvitch, M. A. Washington, H. A. Huggins, and J. M. Rowell, IEEE Trans. Magn. **MAG-19**, 791 (1983).
[16] P. Verhoeve, N. Rando, A. Peacock, A. van Dordrecht, D. Lumb, D. J. Goldie, and R. Venn, Nucl. Instrum. Methods Phys. Res. A **370**, 136 (1996).
[17] P. A. J. de Korte, Proc. ESA Symp. **SP-356**, 41 (1992).
[18] A. Rothwart and B. N. Taylor, Phys. Rev. Lett. **19**, 27 (1967).
[19] P. Verhoeve, N. Rando, A. Peacock, A. van Dordrecht, A. Poelaert, and D. J. Goldie, IEEE Trans. Appl. Supercond. **7**, 3359 (1997).
[20] A. A. Golubov, E. P. Houwman, J. G. Gijsbertsen, J. Flokstra, H. Rogalla, J. B. le Grand, and P. A. J. de Korte, Phys. Rev. B **49**, 12 953 (1994).
[21] S. B. Kaplan, C. C. Chi, D. N. Langenberg, J. J. Chang, S. Jafarey, and D. J. Scalapino, Phys. Rev. B **14**, 4854 (1976).
[22] A. Poelaert, A. A. Golubov, P. Verhoeve, A. Peacock, and H. Rogalla, Phys. Rev. B (submitted).
[23] K. E. Kihlstrom, R. W. Simon, and S. A. Wolf, Physica B & C **135B**, 198 (1985).